PRODUCTION PROCESS

Evaluation of residual stress development in FRP-metal hybrids using fiber Bragg grating sensors

R. Prussak[1] · D. Stefaniak[2] · C. Hühne[2] · M. Sinapius[1]

Abstract

This paper presents experimental measurement methods for the determination and evaluation of process related thermal residual stresses in fiber metal laminates. A cure monitoring system with fiber Bragg grating (FBG) sensors is used to measure the in-plane strains during processing of carbon fiber reinforced plastic (CFRP)-steel laminates. The simultaneous measurement captures the thermal expansion during the heating stages, the cure shrinkage, and the cooling thermal shrinkage. The results enable the characterization of the co-cure bonding process and the stress transfer between the metal and FRP-layers during the creation process. The residual strains, which are used for calculation of the residual stresses, are recorded at room temperature after manufacturing. In addition, an advanced method using FBG-sensors and the deflection of asymmetric hybrid specimens is developed to validate the gained residual stress data. Asymmetrical specimens are created by removing selected layers after cure. Quantitative evaluation is achieved by determination of their curvature and measuring the strain changes with the embedded FBG-sensors. For validation, the methods were successfully demonstrated on two different curing cycles with different resulting residual stress levels. The simultaneous strain measurement enables the investigation of stress development and delivers more in-depth process knowledge for further optimization of the manufacturing process.

Keywords Fiber metal laminate · Residual stress · Co-cure bonding · Process monitoring · FBG

1 Introduction

Fiber metal laminates (FML) are hybrid composite materials consisting of metal sheets co-cure bonded to fiber reinforced plastic layers (FRP). No additional joining process is needed as adhesion is realized by the resin during its cure [1–3]. The resulting properties of the hybrid material need to be predictable when used in structural applications. In addition to its constituents, their composition and bonding as well as their manufacturing history and the resulting residual stresses play an important role [4–10].

Residual thermal stresses occur as a consequence of the difference in the coefficients of thermal expansion (CTE) of the two constituents and the difference between cure temperature of the matrix and operational temperature of the cured laminate. They are mainly affected by the thermal expansions of the different components and the chemical shrinkage of the plastic, which are influenced by a variety of extrinsic and intrinsic parameters [6]. Intrinsic parameters are material properties, lay-up configurations and the total volume ratio of metal to composite. Extrinsic parameters are process and tooling related parameters. Different investigations have been performed to affect residual stresses by modifying these parameters, utilize modifications in curing process [7, 8], using an additional clamping tool [9] or a post stretching of the cured laminate [10]. Furthermore geometrical effects, like spring-in, tool part interaction, like warpage and forced interaction as well as interply interactions could affect the residual stresses [11–13]. Therefore, the resulting residual stress state is a complex combination of many different parameters, which requires further investigations.

Depending on the constituent's fraction and stiffness, these stresses may significantly lower the mechanical properties of the hybrid laminate, especially when difference in thermal expansion is high. Difficulties in precisely determining residual stresses often lead to conservative prediction, which result in heavier structures. Thus it is important to

✉ R. Prussak
r.prussak@tu-braunschweig.de

1 Institute of Adaptive Systems and Functional Integration, TU-Braunschweig, Brunswick, Germany

2 Institute of Composite Structures and Adaptive Systems, German Aerospace Center (DLR), Brunswick, Germany

investigate methods to determine residual stresses. In addition, a clear understanding of how process-induced strains evolve during the cure cycle could help to optimize manufacturing. This can only be achieved by a simultaneous measurement method.

Therefore, a cure monitoring system with fiber Bragg grating (FBG) sensors is used to measure the in-plane strains during processing of FRP-metal hybrids. Fiber optic sensors were integrated directly into CFRP-steel laminates and provide information about the strains and the residual stress state.

The laminate`s lay-up is based on a unidirectional (UD)-CFRP-steel laminate where UD-CFRP layers are combined with steel layers in a way that the laminate contains only one fiber direction [14]. In contrast, four fiber directions are used in aerospace applications due to the damage tolerance requirements. Thus, when used for mainly unidirectionally loaded parts, an essential proportion of the CFRP's capability remains unused to fulfill residual-strength-after-impact requirements. In a UD-CFRP-steel laminate the steel layers substitute three fiber directions and, hence, the laminate stiffness and strength in 0°-direction are not reduced while residual-strength-after-impact is improved compared to pure unidirectional laminates [15].

On the other hand, the high stiffness, low metal volume fraction and large difference in the thermal expansion coefficients lead to very high internal residual stresses [6].

2 Fundamentals

When measuring processing strains, it is necessary to identify the different influencing parameters on the sensor signal in detail. Therefore, a calibration of the bare fiber Bragg sensors is carried out. The experimentally determined temperature sensitivity is required for the temperature compensation during the curing process.

2.1 Function

Fiber Bragg grating (FBG) sensors can operate as wavelength-encoded sensors and provide an absolute measurement of the physical perturbation which they experience [16]. The sensor is sensitive to strain-, temperature- or pressure changes and can be directly integrated into FRP-laminates to monitor the processing strains during the curing process [17–19]. In addition, stresses can also be measured after finishing the manufacturing process. This allows the determination of the combined stress state from the manufacturing process and the application.

The Bragg grating is a periodical modulation of the refractive index, photo-written in the core of a single mode optical fiber, with a spread of a few millimeters. When the fiber is strained by ε or submitted to a temperature change ΔT, a shift $\Delta\lambda_b/\lambda_b$ of the Bragg wave-length (back reflected wavelength) occurs due to a change of the period of the grating and the refractive index [20]:

$$\frac{\Delta\lambda_b}{\lambda_b} = C_T \times \Delta T + C_S \times \varepsilon, \tag{1}$$

where C_S is the coefficient of strain, which is given as a constant with 0.78 [20]. C_T describes the thermo-optic coefficient, which is related to the change of the refractive index.

2.2 Sensor calibration

When an FBG is used to measure strains, the effect of temperature needs to be calculated. This sensitivity is related to the thermal expansion of the optical fiber and the change of the refractive index:

$$\left[\frac{\Delta\lambda_b}{\lambda_b}\right]_T = \left(C_S \times \alpha_f + C_T\right) \times \Delta T = S_T \times \Delta T, \tag{2}$$

where α_f is the thermal expansion coefficient of the bare glass fiber. The temperature sensitivity S_T of a bare fiber is determined experimentally, as shown in Fig. 1.

Through a linear regression, a value of 6.6 ppm/K can be determined in the temperature range up to 140 °C, which corresponds to results from the literature [17, 19]. After exceeding 140 °C, the temperature sensitivity increases significantly. Over the entire process up to 180 °C, a standard cure temperature for aerospace epoxy systems, an average sensitivity of 6.9 ppm/K can be determined.

In the case of an embedded sensor, the thermal expansion of the fiber α_f, corresponds to the expansion of the bedding material. Therefore, when an FBG is used to measure processing strains, only the thermo-optic effect of the temperature needs to be compensated. Thus the fiber optical measurement
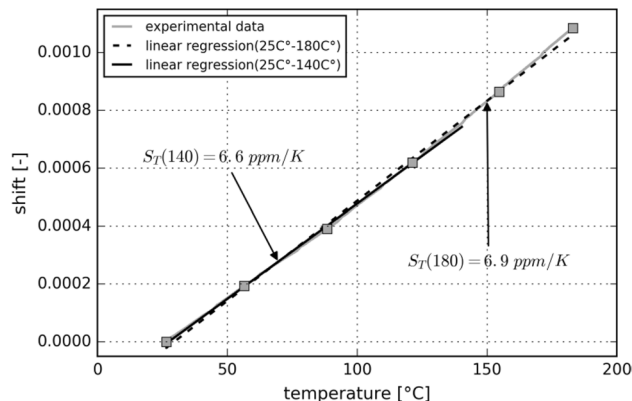

Fig. 1 Temperature sensitivity of the FBG-sensor

method allows the calculation of a full strain profile during the process with the following equation:

$$\varepsilon_p = \frac{\frac{\Delta \lambda_b}{\lambda_b} - \left(C_T \times \mathbf{\Delta T} \right)}{C_S}. \tag{3}$$

The thermo-optic coefficient of the temperature is calculated by changing formula (2) to:

$$C_T = S_T - C_s \times \alpha_f. \tag{4}$$

The thermal expansion of the optical fiber (quartz glass) α_f is given as 0.54 ppm/K [21]. This results in a thermo-optic coefficient C_T of 6.2 ppm/K for temperature applications up to 140 °C and 6.5 ppm/K for applications up to 180 °C.

2.3 Sensor validation

The measured in-plane strains during processing of a CFRP laminate are very small due to the high stiffness and low thermal expansion of the fibers. This results in a very high temperature sensitivity of the results. Therefore, the experimentally determined and assumed values are validated with an additional experimental setup shown in Fig. 2, which simulates the behavior of the fiber in the embedded case under temperature load. The Bragg grating is located in the middle of the cut-out. The temperature of the steel ring T_s and the air temperature at the sensor T_a are recorded. The experiment separates the effects of the thermal expansion of the base material and the thermo-optic coefficient.

The whole setup is heated up in an oven. There are different temperature profiles of T_s and T_a over time. The change of the reflected wavelength can be determined by the following equation:

$$\left[\frac{\Delta \lambda_b}{\lambda_b} \right]_T = C_S \times \alpha_s \times \mathbf{\Delta T_s} + C_T \times \mathbf{\Delta T_a}, \tag{5}$$
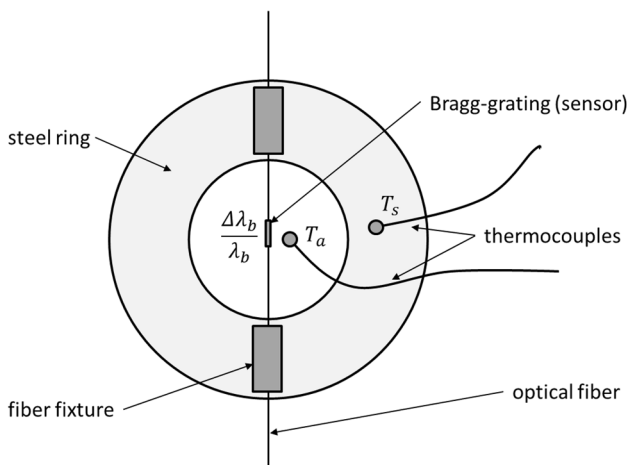
where α_s is the thermal expansion coefficient of the steel ring (S235JH), which is given as 11.1 ppm/K [23]. In Fig. 3 the measured temperature profiles and the wavelength shifts are shown. In comparison, the calculated shift with formula (5) is presented.

The calculated shift curve shows good agreement to the measured shift up to the measured 1800s. Therefore, a correct determination of the characteristic values of the used FBG-sensor can be assumed. The determined characteristic values and the procedure for the temperature compensation form the basis for the further investigations.

3 Residual stress determination

In this paper two methods are presented for the determination of the residual stresses in fiber metal laminates using FBG-sensors.

3.1 Simultaneous measurement of processing strains

The fiber optical measurement method records a processing strain profile during the complete process. The strain data is based on the point of gelation, where the strain data is set zero. The residual strains, which were used for calculation of the residual stresses, are recorded at room temperature after finishing manufacturing.

Using the classical laminate theory (CLT) approach, an apparent thermal load n can be calculated from the measured process strain ε_p and the stiffness matrix A of the laminate:

$$\{n\}_T = [A] \times \{\varepsilon_p\}. \tag{6}$$

The temperature and strain are considered constant over the thickness of the laminate. With the help of the thermal load n and the thermal expansion coefficient of the complete
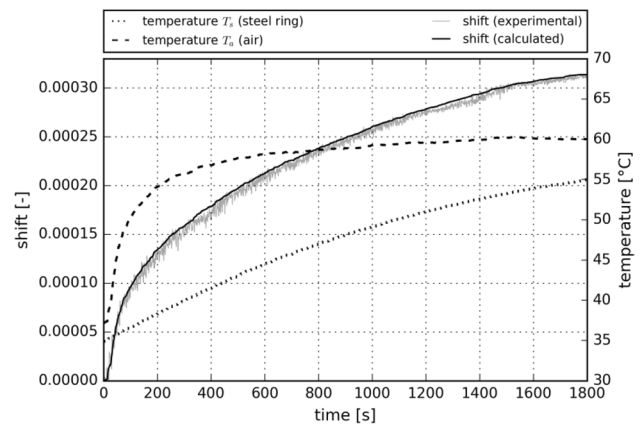

Fig. 2 Experimental setup for sensor calibration

Fig. 3 Comparison between measured and calculated shift

laminate α_T, a temperature change ΔT can be calculated from:

$${n}_T = [A] \times \{\alpha_T\} \times \Delta T. \tag{7}$$

Thus, the residual stresses σ_r in the individual layers can be determined with the thermal expansion coefficient α_t of each layer k with the following equation:

$${\sigma_r}_k = [Q]_k \times (\{\varepsilon_p\} - \{\alpha_t\} \times \Delta T)_k, \tag{8}$$

where Q represents the stiffness matrix of each layer.

3.2 Subsequent uncovering of defined layer stacks

An additional method using FBG-sensors and the deviation of asymmetrical hybrid specimens is developed to validate the gained residual stress data. The procedure is presented schematically in Fig. 4. The exemplary hybrid laminate consist of two FRP layers with one metal center layer. The FBG-sensors are integrated in 0° and 90° direction in the top FRP layer. Step 1 shows the curing process, where the processing strains ε_p can be measured at room temperature. These strains are used for the calculation of the residual stress, presented in Sect. 3.1.

Step 2 is an uncovering process at room temperature. Asymmetrical specimens are created by removing certain layers after cure. The curvature is calculated by the measured geometrical values a and S at room temperature. The assumption of a bimetallic strip allows calculating the stress-free temperature of the radius with the formula provided by Timoshenko [23]. With the help of the calculated temperature, the internal residual thermal stress on the metal layers in fiber direction is evaluated based on classical laminate theory, described in Sect. 3.1.

Besides the information of the deformation of the asymmetrical specimens, there is a strain change in the removed

Fig. 4 Schematic uncovering process of defined layer stacks

FRP-layer during the separation of the asymmetrical part, which is measured by the FBG-sensors. The recorded strain changes ε_f correspond to the released residual strains. The residual stresses σ_r in the FRP layer F can be determined by Hooke's law with:

$$\{\sigma_r\}_F = [Q]_F \times \{\varepsilon_f\}_F. \tag{9}$$

The assumption of equilibrium of forces within the laminate is expressed by:

$$A_M \times \{\sigma_r\}_M + A_F \times \{\sigma_r\}_F = 0. \tag{10}$$

A_M and A_F represent the cross-sectional areas of steel and CFRP layers, while $\{\sigma_r\}_M$ represents the stress in the metal layer, which is calculated by:

$$\{\sigma_r\}_M = -\frac{\{\sigma_r\}_F \times A_F}{A_M}. \tag{11}$$

The method allows the quantitative determination of residual stresses independent of the definition of the point of gelation. The information about curvature and strain can be used to validate the residual strain measurement during cure. The method can also be applied to monolithic fiber composite laminates.

The subsequent removal of defined layer stacks can be carried out by peeling processes or by a milling operation. In the following tests, separation films are inserted in the edge areas (10 mm), which enables specific layers to be peeled off after the process.

4 Experimental testing

The presented methods are used for the evaluation of residual stresses in UD-CFRP steel laminates. Identical specimens with embedded FBG-sensors were manufactured with two different cure cycles. In addition, a sensor is integrated into a monolithic UD-CFRP laminate to determine the influence of resin kinetics on the formation of residual stresses.

4.1 Experimental setup

As manufacturing is part of the investigation, specimens are not cut out of a plate but directly manufactured individually at final geometry. All specimens are 100 mm in width and have a length of 200 mm with all fibers orientated in longitudinal direction (0°).

The schematic lay-up is shown in Fig. 5. The hybrid laminate $[0_3|Stl|0_6]_S$ consist of two stainless steel 1.4310 sheets with a thickness of 0.12 mm and 18 HexPly-8552/AS4 prepreg layers with a thickness of 0.125 mm, each. The
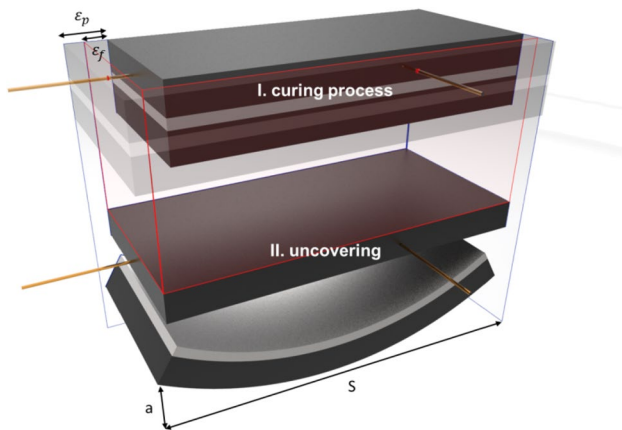
Fig. 5 Specimen geometry and lay up ($l = 200$ mm, $w = 100$ mm, $h = 2.5$ mm)
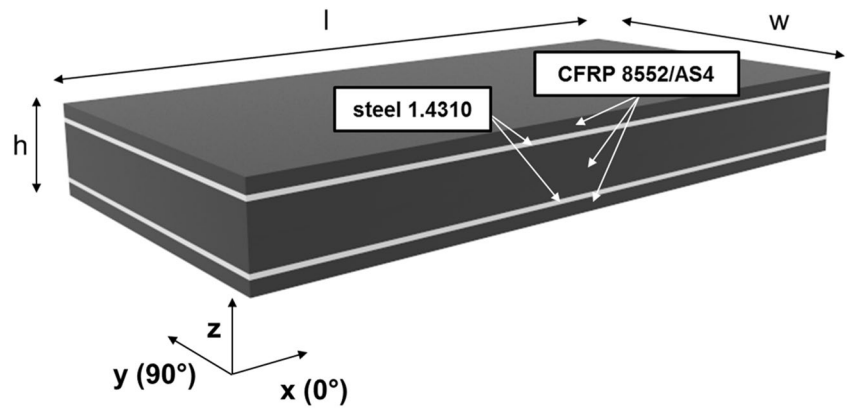
Table 1 Material data [24, 25]

Property	Steel 1.4310 [24]	CFRP 8552/AS4 [25]	Unit
	Value	Value	
E_1	165	131.6	GPa
E_2	186	9.2	GPa
G_{12}	71	4.8	GPa
v_{12}	0.3	0.318	–
α_1	16.4	0.13	ppm/K
α_2	16.4	37.12	ppm/K

Fig. 6 Temperature curve of the modified curing cycle

metal volume fraction (MVF) is 9.6% resulting in a total thickness of 2.49 mm. The monolithic CFRP specimen $[0_{20}]$ consists of 20 HexPly-8552/AS4 prepreg layers with a total thickness of 2.50 mm. The material data is shown in Table 1.

All metallic sheet surfaces were treated with an AC-130 sol–gel post-treatment after corundum-blasting with 105 μm particles. The grits are conducted parallel to the metal foil surface. A turbulent motion of the grits achieves a mild abrasion and removal of the substrate. With the help of an automated facility, the material's feed rate and the grit flow can be controlled to guarantee consistent process conditions [3]. The process proved to be reliable and provides comparably high shear strength values when comparing to chemical and conventional grit-blasting pre-treatments [15].

The standard cure process is defined by the manufacturer's recommended cure cycle (MRCC) with a pressure of 6 bar. MRCC for the HexPly-8552/AS4 prepreg recommends two heat-up ramps and two dwell stages. The hybrid laminate is heated up to 110 °C at 2 K/min. After the 60 min dwell it is heated up again at 2 K/min to 180 °C. After a hold of 120 min it is cooled down at 2–5 K/min. In this investigation the process is carried out in an oven. Thereby, no additional pressure is applied.

A modified curing cycle with cooling and reheating, which generates a different residual stress state, is used to validate the measurement methods (Fig. 6). The cooling
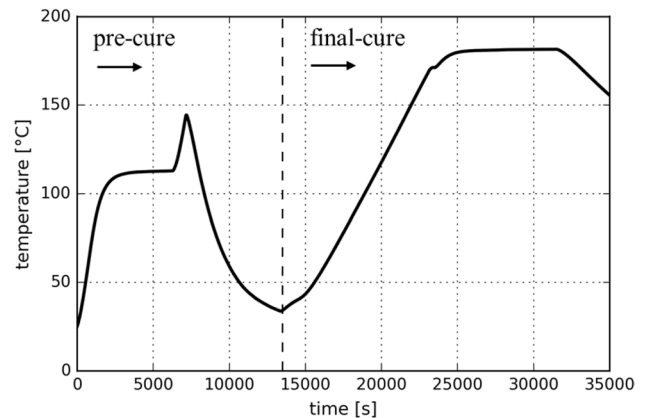
takes place during the second dwell. Then, after reaching a temperature around 60 °C, the reheating up to the curing temperature of 180 °C begins. The aim of modified cure cycles is to lower the bonding temperature of CFRP—and steel layers. This is based on the exothermic curing reaction which proceeds during the abrupt cooling. As a consequence, the connection between steel and prepreg solidifies at a lower temperature [7, 8, 18].

For the experimental investigations of the residual stresses a polyimide coated silica glass FBG-sensor is embedded in the described CFRP-steel laminates. The optical fibers are longitudinally (0°) and transversally (90°) placed between the center layers. Figure 7 shows the crossply section of the hybrid laminate with the embedded sensor. The Bragg grating (sensor) is in the middle of the length and width of the samples. In addition, the temperature during the curing process is recorded with embedded K-Type thermocouples. The gauge length of the Bragg grating is 2 mm. The outside diameter, including the polyimide coating, is about 150 μm.

The variation of the reflected light wavelength by the FBG during curing in an oven is monitored using an optical sensing interrogator, whose wave-length range is 40 nm. The interrogator operates as light source and spectrometer. The
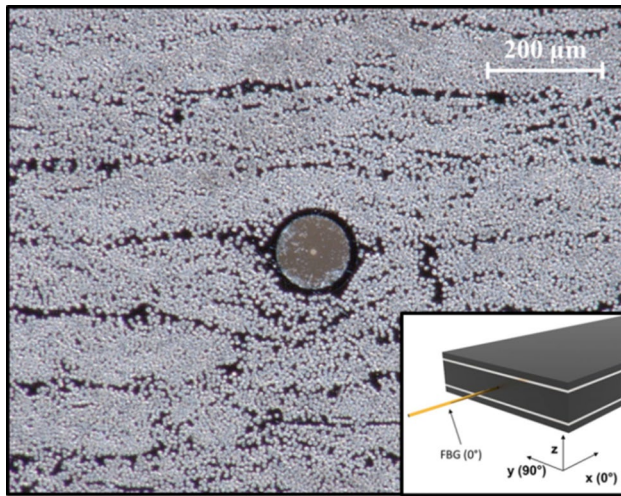
Fig. 7 Micrographics of CFRP-steel laminate with embedded FBG-sensor in longitudinal direction (0°)

exact wave-length shift can be determined by a peak detection of the reflected wavelength band. Both, temperature and wavelength change were measured with a sampling rate of 1 Hz.

4.2 Residual stress results

Figure 8 shows the strain for the pure CFRP laminate in transverse (90°) direction during the curing process (MRCC) and describes the behavior of the resin through its several phases. The observed sudden change in slope is a result of the cure shrinkage, which occurs when the material transforms from a liquid to a rubbery state. The resin gels, as confirmed through different investigations in the literature using in-situ strain measurements during processing [26–28]. This allows the determination of the point of gelation at
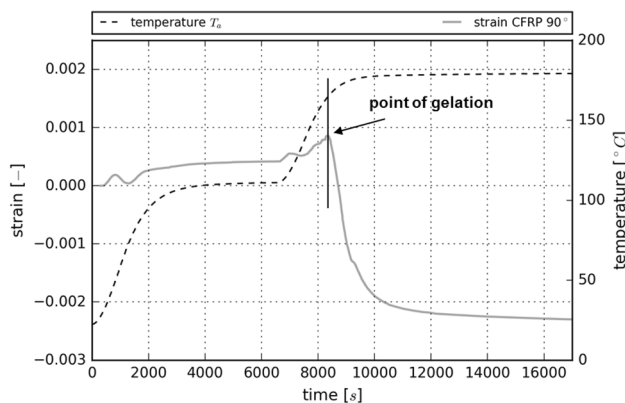
a temperature of 163.5 °C, which is consistent with other investigations on the 8552-epoxy system with a heating rate in the test of around 2.5 K/min [26, 29].

The measured strains in transverse and longitudinal direction during the curing process of the CFRP-steel laminate are shown in Fig. 9.

A characteristic peak is seen in longitudinal direction. In contrast to the CFRP in 90° direction, the shrinkage after gelation is restricted through the stress transfer between the matrix, carbon fibers and steel layers. This results in a very small peak followed by a further increase due the thermal expansion.

A characteristic peak cannot be detected in the transverse direction. The shrinkage is overcompensated through the thermal expansion of the steel layers, because of the low stiffness of the UD-CFRP prepreg layers in transverse direction. As a result, the measured strains increase significantly until the constant cure temperature is reached and are then followed by shrinkage induced decrease.

Figure 10 presents the strain in transverse direction as function of the temperature. It shows the strain development during transformation of the matrix from a liquid to a rubbery state. Before gelation, the curve has only a very small increase. The resin is in a liquid state, therefore, no significant stresses between the metal - and CFRP layers can be transferred. During the gelation the slope of the curve sharply increases due to the starting interaction between the layers. The coefficient of thermal expansion (CTE) after gelation of the hybrid laminate reaches nearly the same value as during cooling down.

Consequently, the cure kinetic, especially the point of gelation, has a significant influence on the development of residual stresses. Exact knowledge of the influencing parameters and their effects on the curing process can help to adjust the co-cure bonding process [30]. In addition, the measuring method using FBG-sensors can be used to
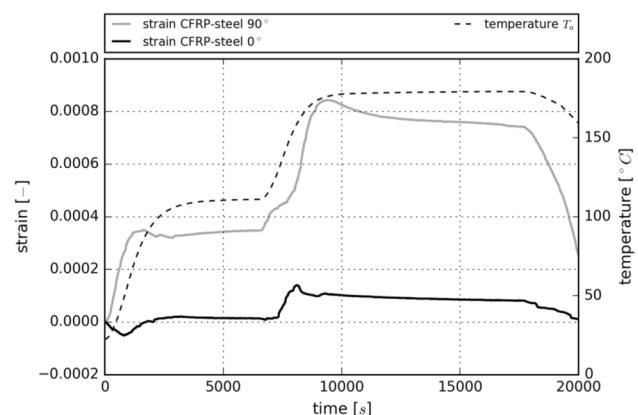

Fig. 8 Measured strains (in 90° direction) during the curing process (MRCC) of a UD-CFRP $[0_{20}]$ laminate

Fig. 9 Measured strains (0°- and 90°-direction) during the curing process of a CFRP-steel laminate $[0_3|St|0_6]_S$
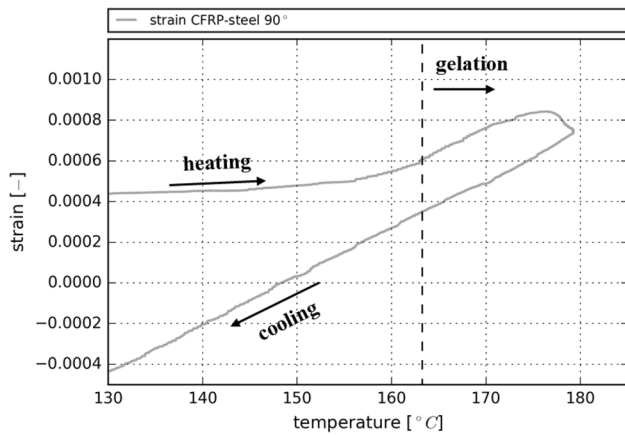
Fig. 10 Measured strain (90°-direction) as a function of the temperature during the curing process of a CFRP-steel laminate $[0_3|St|0_6]_S$
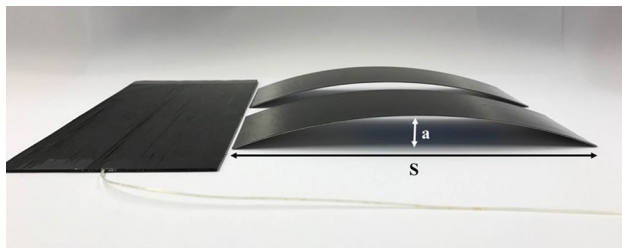

Fig. 12 Measured strains (0°- and 90°-direction) during the uncovering process of a CFRP-steel laminate

Fig. 11 Uncovered UD-CFRP laminate with removed asymmetrical hybrid specimens

Fig. 13 Comparison between the released strains during uncovering in 0°-direction for the standard (MRCC) and modified (MOD) cure cycle

develop a direct correlation between the cure kinetics and the residual strains. This allows further process optimization to reduce residual stresses.

The point of gelation is defined as stress-free and all strain plots were set to zero at this point. At room temperature and after demolding, the residual strain ε_{p0} in 0°-direction can be determined with 0.00033 and ε_{p90} in 90°-direction with 0.00328.

For the recording of the residual strains independent of the definition of the gel point, the presented uncovering method is used. The mechanical removing (peeling) of the outer steel and CFRP layers after manufacturing process at room temperature results in a UD-CFRP laminate $[0_{12}]$ and two asymmetrical hybrid specimens $[0_3|St]$ (Fig. 11). The strain data during the uncovering of the standard cured hybrid laminate is presented in Fig. 12.

It clearly shows the removal of the bottom at 400 s and top asymmetrical steel-CFRP layer stack at 850 s with a sudden change in strain. The CFRP layers are under a compressive - and the metal layers are under a tensile stress in 0°-direction after finishing the manufacturing process. There is the exactly reversed stress state in 90°. Thus, the strain in the CFRP layers decreases in transverse direction and
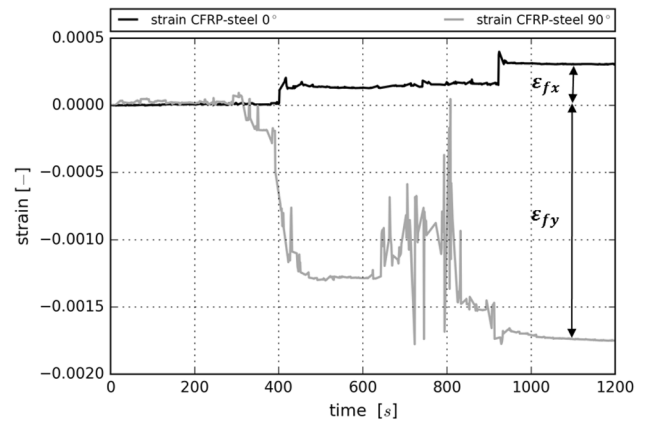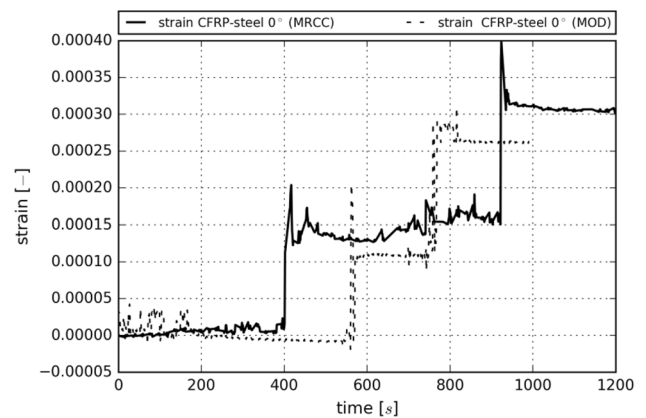
rises in longitudinal direction. The strain change reflects the elimination of the forced expansions. The resulting UD-CFRP laminate $[0_{12}]$ contains no more restricted interlaminar strains. Thus, the residual stress state can be determined from the strain change through the removal of the defined layer stacks. The measured residual strain ε_{fx} in 0°-direction is 0.0003 and ε_{fy} in 90°-direction is -0.0018.

Figure 13 shows the comparison between the released strains during the uncovering procedure in 0°-direction for the standard (MRCC) and modified (MOD) cure cycle. The strain in the 0°-direction for the modified cycle is significantly lower with 0.00026 than for the standard process.

By recording the length S and the deflection a, which are shown in Fig. 11, the curvature can be calculated with the assumption of uniform deformation. The result is a radius of 196.7 mm for the standard process with a maximum deflection of 22.5 mm and a radius of 235.4 mm for the modified cycle with a maximum deflection of 18.9 mm.

Fig. 14 Comparison between the curvature of the removed asymmetrical specimens [0₃|St] for the standard (MRCC) and modified (MOD) cure cycle
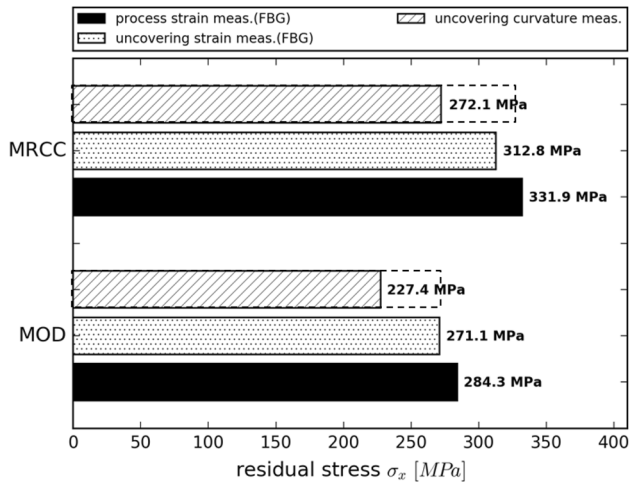

Fig. 15 Residual stress results with the different measurement methods for the standard (MRCC) and modified (MOD) cure cycle

Figure 14 shows the significantly lower deformation of the modified cured sample.

The residual stresses can be calculated by using the measured processing strains ε_p in formula (8) and the released strains ε_f in the formula (9) as well as the curvatures of the separated asymmetric samples in the formula of the bi-material strip by Timoshenko [23], taking into account the material data from Table 1.

The results of the different methods for the standard and the modified manufactured CFRP-steel laminate are presented in Fig. 15. The values shown describe the normal stress of the metal layers in the longitudinal direction. The measurement methods with the FBGs show similar results. The curvature measurement shows a somewhat lower residual stress level. This could already be shown in previous studies, where the curvature measurement shows around 20% lower residual stresses as the direct measurement of the stress-free temperature during reheating of the curved asymmetrical specimens [6]. The curvature measurement with the offset of 20% is shown as dashed lines in Fig. 14. This results in nearly the same stress lever for all three measurement methods.

However, the stress change between the standard and the modified cycle are almost the same for all measurement procedures. The process strain measurement shows a stress reduction of 47.6 MPa, the uncovering strain measurement 41.7 MPa and the uncovering curvature measurement 44.7 MPa. This enables a very exact evaluation of the influence of modifications during the processing on the residual stress state.

5 Conclusion

In this work a residual stress measurement method using fiber Bragg grating sensors is presented and applied to fiber metal laminates. For an exact determination of the processing strains, a calibration of the bare fiber Bragg sensors is carried out. A new method is used to successfully validate the experimentally determined sensitivity of the sensor as well as the procedure of temperature compensation during processing. In-situ strain monitoring during the manufacturing process of CFRP-steel laminates are performed. The relationship between curing reaction and the measured strains can be clearly detected. The technique captures the thermal expansion and the cure shrinkage during the heating stage and allows the determination of the gelation and the starting interaction between the metal and FRP layers. The recording of the strains after the curing process and demolding enables the determination of the residual stress level by using the CLT approach. In addition, a method for determining the residual stresses, independent of the definition of the point of gelation and also without temperature and pressure influences on the sensor signal, is developed. The methods could be successfully carried out for two different processes with different residual stress levels. Both measuring methods show a good agreement of the residual stress results. The change in residual stress due to the modification of the process can be demonstrated almost equally by all methods.

FBG-sensors show the potential to determine residual stresses in hybrid laminates. Furthermore, the simultaneous strain measurement enables the evaluation of the stress development during cure. This allows the determination of influencing process parameters on the behavior of the curing strains and the resulting stress level. The investigations form the basis for a targeted adjustment of process parameters to minimize process-related residual stresses in so-called "smart cure cycles".

References

1. Sinmazcelik T, Avcu E, Bora M, Coban O (2011) A review: fibre metal laminates, background, bonding types and applied test methods. Mater Des 32(7):3671–3685

2. Van Roojnen R, Sinke J, De Vries TJ, Van Der Zwaag S (2004) Property optimisation in fibre metal laminates. Appl Compos Mater 11(2):63–76

3. Koch SF et al (2016) Intrinsic hybrid composites for lightweight structures: new process chain approaches. Adv Mater Res 1140:239–246

4. Chandrasekar M, Ishak MR, Jawaid M, Leman Z, Sapuan SM (2017) An experimental review on the mechanical properties and hygrothermal behaviour of fibre metal laminates. J Reinf Plast Compos 36(1):72–82

5. Yu Y, Ashcroft IA, Swallow G (2006) An experimental investigation of residual stresses in an epoxy-steel laminate. Int J Adhes Adhes 26:511–519

6. Stefaniak D, Kappel E, Kolotylo M, Hühne C (2014) Experimental identification of sources and mechanisms inducing residual stresses in multi-layered fiber-metal-lamiates. Euro Hybrid Materials and Structures, Stade

7. Kim HS, Park SW, Hwang HY, Lee DG (2006) Effect of the smart cure cycle on the performance of the co-cured aluminium/composite hybrid shaft. Compos Struct 75(1–4):276–288

8. Kim HS, Park SW, Lee DG (2006) Smart cure cycle with cooling and reheating for co-cure bonded steel/carbon epoxy composite hybrid structures for reducing thermal residual stress. Compos Part A Appl Sci Manuf 37(10):1708–1721

9. Xue J, Wang WX, Takao Y, Matsubara T (2011) Reduction of thermal residual stress in carbon fiber aluminum laminates using a thermal expansion clamp. Compos Part A Sci Manuf 42(8):986–992

10. Khan SU, Alderliesten RC, Benedictus R (2009) Post-stretching induced stress redistribution in Fibre Metal Laminates for increased fatigue crack growth resistance. Compos Sci Technol 69(3–4):396–405

11. Stefaniak D, Kappel E, Spröwitz T, Hühne C (2012) Experimental identification of process parameters inducing warpage of autoclave-processed CFRP parts. Compos Part A Appl Sci Manuf 43(7):1081–1091

12. Twigg G, Poursartip A, Fernlund G (2015) An experimental method for quantifying tool-part shear interaction during composite processing. Compos Sci Technol 63(13):1985–2002

13. Kappel E, Stefaniak D, Fernlund G, Predicting process-induced distortions in composite manufacturing—a pheno-numerical simulation strategy. Compos Struct, 120:98–106

14. Fink A (2010) Lokale Metall-Hybridisierung zur Effizienzsteigerung von Hochlastfügestellen in Faserverbundstrukturen, PhD thesis, German Aerospace Center (DLR), Institute of Composite Structures and Adaptive Systems, Braunschweig

15. Stefaniak D, Kappel E, Kolesnikov B, Hühne C (2012) Improving the mechanical performance of unidirectional CFRP by metal-hybridization. In: ECCM15—E15th European Conference on Composite Materials, Venice

16. De Oliveira R et al (2008) Experimental investigation of the effect of the mould thermal expansion on the development of internal stresses during carbon fibre composite processing. Compos Part A 39(7):1083–1090

17. Mulle M, Collombet F, Olivier P, Grunevald YH (2009) Assessment of cure residual strains through the thickness of carbon–epoxy laminates using FBGs, Part I: elementary specimen. Compos Part A Appl Sci Manuf 40:94–104

18. Kim SS, Murayama H, Kageyama K, Uzawa K, Kanai M (2012) Study on the curing process for carbon/epoxy composites to reduce thermal residual stress. Compos Part A Appl Sci Manuf 43:1197–1202

19. Kang HK, Kang DH, Bang HJ, Hong CS, Kim CG (2002) Cure monitoring of composite laminates using fiber optic sensors. Smart Mater Struct 11:279–287

20. Hill KO, Meltz G (1997) Fiber Bragg grating technology fundamentals and overview. J Light Technol 15(8):1263–1276

21. Heraeus (2014) Base materials—Heraeus Quarzglas—product data

22. ThyssenKrupp Materials International (2011) S235JXX—Product Data

23. Timoshenko S (1925) Analysis of Bi-Metal thermostats. J Opt Soc Am 11(3):233–255

24. Petersen E, Stefaniak D, Hühne C (2017) Experimental investigation of load carrying mechanisms and failure phenomena in the transition zone of locally metal reinforced joining areas. Compos Struct 182:79–90

25. Marlett K (2011) Hexcel 8552 AS4 Unidirectional Prepreg at 190 gsm & 35% RC Qualification Material Property Data Report. NCAMP Test Report, Revision A

26. Garstka T, Ersoy N, Potter KD, Wisnom MR (2007) In situ measurements of through-the-thickness strains during processing of AS4/8552 composite. Compos A 38:2517–2526

27. Hua H, Li S, Wang J, Zu L, Cao D, Zhong Y (2017) Monitoring the gelation and effective chemical shrinkage of composite curing process with a novel FBG approach. Compos Struct 176:187–194

28. Minakuchi S (2015) In situ characterization of direction-dependent cure-induced shrinkage in thermoset composite laminates with fiber-optic sensors embedded in through-thickness and in-plane directions. J Compos Mater 49(9):1021–1034

29. Ersoy N, Garstka T, Potter K, Wisnom MR, Porter D, Clegg M, Stringer G (2010) Development of the properties of a carbon fibre reinforced thermosetting composite through cure. Compos Part A Appl Sci Manuf 41(3):401–409

30. Studer J, Dransfeld C, Masania K (2016) An analytical model for B-stage joining and co-curing of carbon fibre epoxy composites. Compos Part A Appl Sci Manuf 87:282–289